Fusion Engineering and Design 220 (2025) 115375

Contents lists available at ScienceDirect

Fusion Engineering and Design

journal homepage: www.elsevier.com/locate/fusengdes

Thermal-hydraulic analysis of WCLL BB First-Wall mock-up in Water Loop facility under transient conditions

G. Mongiardini [a,*], A. Vannoni [b], C. Ciurluini [a], P. Maccari [b], B. Gonfiotti [b], P. Arena [b], M. Eboli [b], F. Giannetti [a], A. Del Nevo [b]

[a] DIAEE Department, Sapienza University of Rome, Roma 00186, Italy
[b] Department of Nuclear, Experimental Engineering Division, ENEA, Camugnano, BO 40032, Italy

ARTICLE INFO

Keywords:
DEMO
ITER
WCLL breeding blanket
TBM
Water Loop
RELAP5 code

ABSTRACT

The EUropean DEMOnstration Power Plant (EU-DEMO) represents a milestone in nuclear fusion research, serving as crucial step towards the realization of commercial fusion energy production by bridging the gap between current research efforts and future industrial-scale deployment. A key component of the reactor is the Breeding Blanket (BB) that must perform several essential functions for the proper DEMO operation. Two primary concepts for BB have been proposed for DEMO: the Water Cooled Lithium Lead (WCLL) and the Helium Cooled Pebble Bed (HCPB). Both concepts are going to be tested under realistic fusion reactor conditions in ITER, in the form of Test Blanket Modules (TBMs). In this framework, at the ENEA R.C. Brasimone, the construction of an experimental infrastructure called W-HYDRA is ongoing. It is dedicated to the investigation of the water and lithium-lead technologies applied to the fusion research field. As part of the W-HYDRA infrastructure, Water Loop facility will investigate WCLL BB components, such as a First-Wall (FW) test section. The design characteristics and performance of the mock-up will be assessed to provide valuable experimental results in view of DEMO operation. The present paper is focused on the thermal-hydraulic numerical study of the WCLL BB FW test section within Water Loop facility using RELAP5/Mod3.3. Specifically, the study investigates expected operating transients (i.e., pulse-dwell and dwell-pulse transients) and accidental scenarios (i.e., Loss Of Feedwater Accident, LOFA), with the aim of supporting the design phase by providing preliminary results on the Water Loop facility and on the mock-up operation.

Abbreviations

BB	breeding blanket
BU	breeding unit
CHFR	critical heat flux ratio
CHF	critical heat flux
COB	central outboard blanket
ECO	economizer
EB-gun	electron beam-gun
EU-DEMO	EUropean DEMOnstration Power Plant
FW	First-Wall
HCPB	helium cooled pebble bed
HP	high pressure
HS	heat structures
LIFUS5/Mod4	LIthium FUSion 5 Mod 4
LOFA	loss of feedwater accident
LP	low pressure
MFR	mass flow rate
MU	mock-up
NOS	normal operation state
PIE	postulating initiating event
PL	primary loop
P-S HX	primary-to-secondary heat exchanger
PWR	pressurized water reactor
RC	research center
S-T HX	secondary-to-tertiary HX
SL	secondary loop
SYS-TH	SYStem Thermal-Hydraulic
TBM	test blanket module
TH	thermal-hydraulic
TL	tertiary loop
TS	test section

* Corresponding author.
E-mail address: giorgio.mongiardini@uniroma1.it (G. Mongiardini).

https://doi.org/10.1016/j.fusengdes.2025.115375
Received 13 January 2025; Received in revised form 17 July 2025; Accepted 29 July 2025
Available online 2 August 2025

VC vacuum chamber
WCLL water cooled lithium lead

1. Introduction

In the last decade, the research and development in fusion technology has made significant progress, aiming to demonstrate fusion as a viable energy source. Projects like the ITER experimental reactor [1], and the EUropean DEMOnstration Power Plant (EU-DEMO) [2], have prompted European countries to concentrate their research by establishing EUROfusion [3], a consortium dedicated to advancing nuclear fusion development, bringing together the expertise of leading research institutions and industries.

Among the research efforts in fusion technology a major focus is the development of the Breeding Blanket (BB) [4]. The importance of the BB is related to its main functions: heat removal, tritium breeding, and shielding/protection of the vacuum vessel walls and other components [5]. This protection function is performed through the First Wall (FW), a component facing the plasma, and thus subjected to high heat and neutron loads produced by the fusion reaction. These high-energy neutrons are absorbed by the BB and interact with the lithium contained in the Breeding Units (BUs) generating tritium, which is needed to sustain further fusion reactions. Additionally, the BB regulates thermal flux to ensure efficient capture and conversion of generated energy into usable forms.

The ENEA (Italian National Agency for New Technologies, Energy and Sustainable Economic Development) Brasimone Research Center (R.C.) is an active participant in the EUROfusion consortium. Within this framework, ENEA contributes to the Work Package Breeding Blanket, with a specific focus on Water Cooled Lithium Lead (WCLL) breeding blanket system for the DEMO reactor [6].

To support experimental investigations of water and lithium lead systems and components suitable for this BB option, ENEA is conceptualizing and building a new multipurpose experimental infrastructure called W-HYDRA at the Brasimone R.C [7]. Among the facilities constituting this new platform Water Loop (WL) is designed to investigate WCLL BB components, hosting several mock-ups and testing them with water at Pressurized Water Reactors (PWR) conditions [8].

Some of the experimental campaigns planned for the WL facility focus on the WCLL BB FW, since the proper qualification of this component and the assessment of its cooling capabilities are key issues in the development of an affordable BB design. Therefore, a WCLL BB FW mock-up (MU) was designed with the aim of providing valuable experimental data in view of DEMO operation [9]. Specifically, the tests planned for the WCLL BB FW-MU cover Normal Operation State (NOS), and Loss Of Feedwater Accident (LOFA) condition. The NOS tests have the aim of assessing the FW performances under plasma heat loads during flat-top periods and pulse-dwell operations, whereas the LOFA tests are meant to evaluate the grace time before approaching the maximum allowable temperature for the component, i.e., 550 °C, corresponding to the creep temperature for the FW structural material (plus a safety margin) [6]. Additionally, the tests will provide experimental data for the validation of numerical codes.

In the current paper Thermal-Hydraulic (TH) pre-test analyses of the NOS and LOFA scenarios that will be investigated with the FW-MU are presented. The WL facility and the FW test section were modelled using the SYStem TH (SYS-TH) code RELAP5/Mod.3.3 [10] and sensitivity analysis was performed on the FW-MU nodalization, to optimize its representativeness. Numerical analyses were carried out reproducing the thermal-hydraulic and heat loads conditions that will be obtained during the tests. The aim of the analyses is to provide preliminary insights into the operation of the WL facility and investigate the most suitable control strategy to perform the experimental campaigns. Furthermore, the numerical results obtained characterize the TH performances of the FW-MU design under the simulated NOS and LOFA conditions.

2. Water-Loop facility

Water Loop is part of the W-HYDRA experimental infrastructure that will be built at the ENEA Brasimone R.C. and will also comprise STEAM [11] and LIthium FUSion 5 Mod 4 (LIFUS5/Mod4) [12]. WL is a water facility designed to serve as a test bed for the WCLL BB. Several test sections and mock-ups representative of WCLL BB components will be installed to be characterized from thermal-hydraulic and thermo-mechanical perspectives and to investigate various phenomena. WL is characterized by flexibility and versatility thanks to the use of flanges that hydraulically connect/disconnect the various test sections which can also be positioned inside a Vacuum Chamber (VC), where an 800 kW Electron Beam-gun (EB-gun) simulates the heat flux within the tokamak chamber, thus allowing to assess the performances of high heat flux-heated components.

WL is mainly constituted by three loops.

1. The Primary Loop (PL) is shared with the STEAM facility, and its main aim is to provide PWR conditions to the mock-ups flanged inside or outside the VC. The PL is thermally coupled with the Secondary Loop (SL) by means of a shell-and-tube Primary-to-Secondary Heat Exchanger (P-S HX) and it is equipped with two electrical heaters of 800 kW, with only one working in the WL configuration. The power transferred by the P-S HX is controlled by regulating valves and a dedicated bypass. The main circulation pump is a magnetic-driven centrifugal pump capable of providing a variable mass flow rate (MFR) in the range of 1 to 22 kg/s.
2. The SL is thermally connected with both the PL by the P-S HX, and the Tertiary Loop (TL) by the Secondary-to-Tertiary HX (S-T HX). The SL presents also an Economizer (ECO) installed in the center of the circuit to decrease the thermal stresses on the P-S HX and S-T HX through the reduction of the temperature difference between the tube and the shell side fluids within these components. The circuit can be operated as an 8-shaped loop or an O-shaped loop acting on the isolation valves surrounding the ECO. The design solution opens room for the operation of the PL at temperatures below those envisaged (295 – 328°C)
3. The TL represents the final heat sink for WL. This system is divided into two sections, a section operating at a higher pressure (HP, 0.6 MPa), and another section operating at Low pressure (LP, 0.1 MPa). The latter system is equipped with a cooling tower, which serves as final heat sink.

The WL facility is presented in Fig. 1 and the main parameters of the three loops are listed into Table 1, derived from an updated plant design based on the one described in [8]. The main differences from the previous design are the introduction of the 8-shape at the secondary loop and the separation of the tertiary circuit into two sections.

2.1. WCLL BB First Wall mock-up and test-section design

The DEMO BB is composed by sixteen identical toroidal sectors (22.5 °), each one divided in five poloidal segments (three of outboard and two of inboard blanket segments). These components are constituted by a vertical (poloidal) stack of nearly one hundred breeding cells, that are the system elementary units. Within the cell, two principal BB subsystems can be identified: the breeder zone and the first wall. The reference layout for the latter, optimized during past years of FP8 and FP9 research activities, is fully described in [13,6]. Radially, the FW, represented in Fig. 2 consists of 25 mm of EUROFER, covered by a tungsten layer of 2 mm. Toroidally, it is constituted by a flat plasma facing surface and two elbows that connect it to two radial segments, more properly named side walls. This gives the component a characteristic C-shape. Water flows in squared channels of 7×7 mm^2 with the following thermal-hydraulic conditions: inlet/outlet temperatures of 295–328 °C; reference pressure of 15.5 MPa; velocity field between 3–7

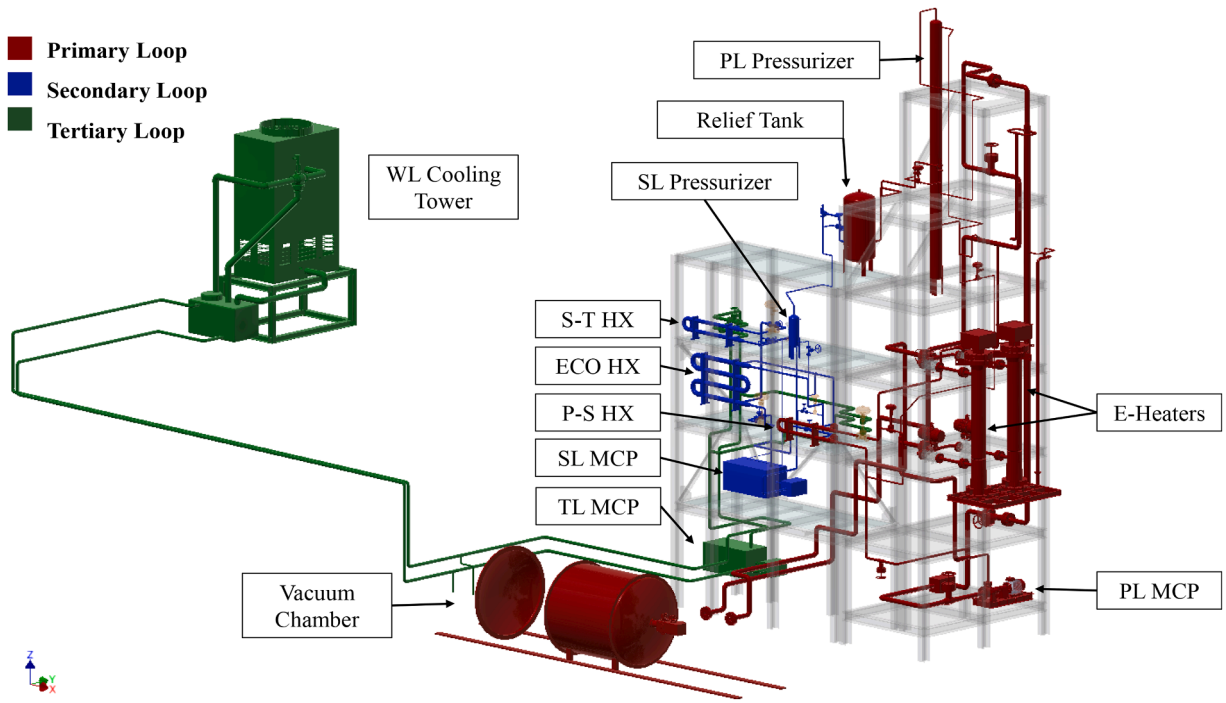

Fig. 1. Overall view of Water Loop facility [8].

Table 1
Main thermal-hydraulic parameters of the WL three loops [8].

Loop TH parameter	PL	SL	TL	
			HP	LP
Working-temperature range	295–328 °C	130–240 °C	50–80 °C	50–53 °C
Design Temperature	360 °C	300 °C	90 °C	90 °C
Nominal Pressure	15.5 MPa	7 MPa	0.6 MPa	0.1 MPa
Design Pressure	18.5 MPa	8.4 MPa	1 MPa	0.2 MPa
Maximum mass-flow rate	20 kg/s	8 kg/s	25 kg/s	28 kg/s

m/s. Channels are located at 3 mm from the plasma facing surface and at 15 mm from the internal surface interfacing the component with the breeder zone. The FW channels follow the C-shape of the component for its whole radial-toroidal-radial extension. They are distributed along the poloidal coordinate. The number of FW channels associated with a single breeding unit varies within each segment and from one segment to another, according to the toroidal-poloidal distribution of the heat flux coming from the plasma. This design solution is obtained by increasing/decreasing the poloidal pitch between adjacent channels.

The FW-MU, shown in Fig. 3, is designed to replicate the plasma-facing section of the WCLL BB FW, thus the flat toroidal section and the two irradiated elbows. However, due to the complexity of the FW

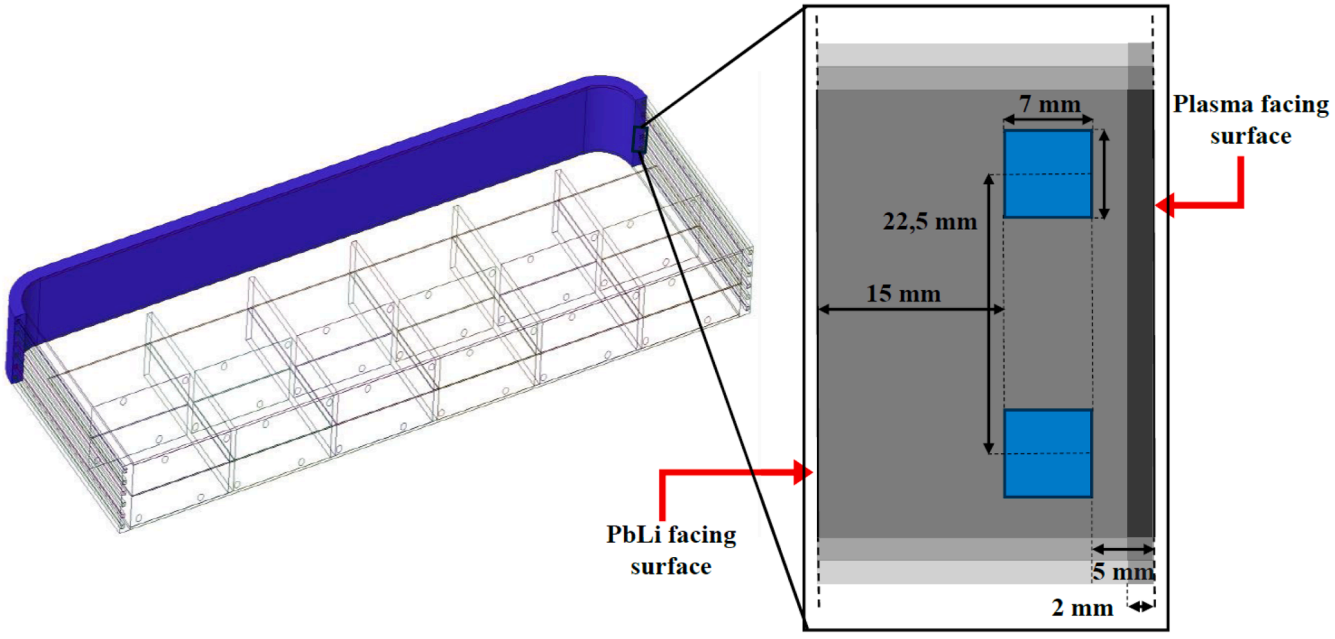

Fig. 2. WCLL BB first wall overview.

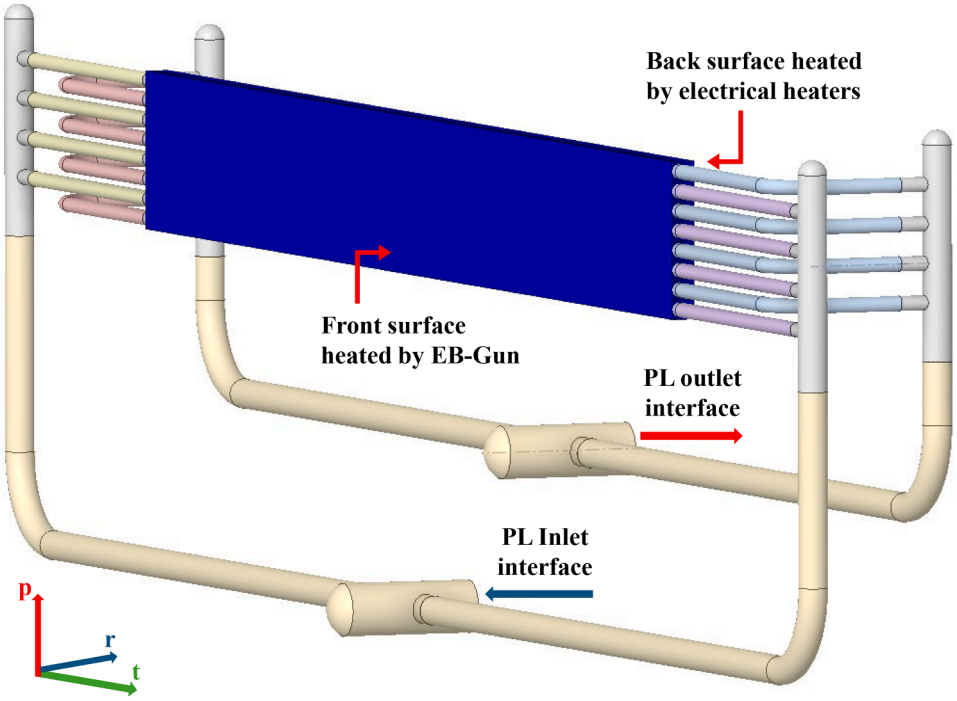

Fig. 3. View of the FW-TS [9].

layout, certain simplifications were made: 1) to enhance manufacturability and reduce costs a straight geometry was chosen, effectively flattening the curved elbows, and 2) the materials will be chosen to closely match the material properties of Eurofer steel [9] and the tungsten coating will not be applied.

Two FW sectors were considered as reference for the design of the FW-MU, the Central Outboard Blanket (COB) at equatorial level, and the COB O7 level, at bottom elevation. For the present analysis the COB O7 level referenced mock-up was considered, being the one subjected to the highest heat flux. FW-MU hosts eight water channels which, compared with the COB O7 level, correspond to one and a half units in the poloidal direction while on the radial direction and channel geometry, it is consistent with the FW layout.

To interface the FW-MU to the WL facility, it was necessary to design a Test Section (TS) that will be flanged to the PL piping inside the VC and will house the FW-MU. As shown in Fig. 3 the TS allows for a first mass flow split, which leads to two inlet manifolds supplying the eight countercurrent channels. Two outlet manifolds collect the mass flow, which is reconnected and directed to the TS outlet. Additionally, a dedicated TS bypass system, equipped with a regulating valve, will be required for the LOFA tests, to divert the appropriate amount of mass flow while working with nominal mass flow rate at the PL pump.

The First-Wall Test Section (FW-TS), placed inside the VC, will be irradiated by means of the EB-gun to simulate the heat flux coming from the plasma. A constant profile will be applied to the central toroidal portion of the FW-MU, while a sinusoidal profile will be used on the lateral sections to simulate the decreasing plasma heat flux on the two elbows. Additionally, the FW-MU will be equipped with electrical back-heaters in order to simulate the fraction of the volumetric heat produced within the lithium-lead in the breeding zone and transmitted to the FW component. The heat fluxes considered in the present analysis are obtained from pre-test CFD calculations performed during the FW-MU design procedure and referring to the nominal working conditions of the COB O7 level FW component [9]. The main dimensions and parameters of the FW-MU and of the TS are presented in Table 2.

Table 2
FW-MU and FW-TS main dimensions and parameters [9].

FW-MU dimensions	
Height (poloidal direction)	180 mm
Length (toroidal direction)	1575 mm
Thickness (radial direction)	27 mm
Front slab (channel-to-front surface distance)	5 mm
Sides of squared channels	7 mm
Back slab (channel-to-back surface distance)	15 mm
N° of channels	8
Channel pitch	22.5 mm
Front and back heated surfaces	0.284 m^2
FW-TS dimensions	
Length (t direction)	2408 mm
Width (r direction)	347 mm
Height (p direction)	618 mm
FW-MU parameters	
EB Gun power (absorbed by the MU)	178.9 kW
Back heaters power	25.5 kW
Maximum EB Gun heat flux	661.6 kW/m^2
Back heaters heat flux	90 kW/m^2
Mass flow rate	1.047 kg/s

3. Pre-test numerical analyses

Thermal-hydraulic simulations of the NOS and LOFA tests were conducted using the RELAP5/Mod3.3 code [10], which allows for a monodimensional representation, through hydrodynamic elements connected by junctions and, where needed, by heat structures (HS). The model replicates the three loops that constitute WL facility, and the WCLL BB mock-up. The nodalization adopted for the WL facility is reported in Fig. 4, while Fig. 5(a) and (b) represent the FW-TS nodalization in the lumped and in the detailed approaches, respectively. The main nodalizaton parameters are reported in Table 3.

The correlation used In RELAP5 to assess the heat transfer coefficient is selected based on the predicted Heat Transfer Mode [14]. In the subcooled liquid region, when the wall temperature is below saturation

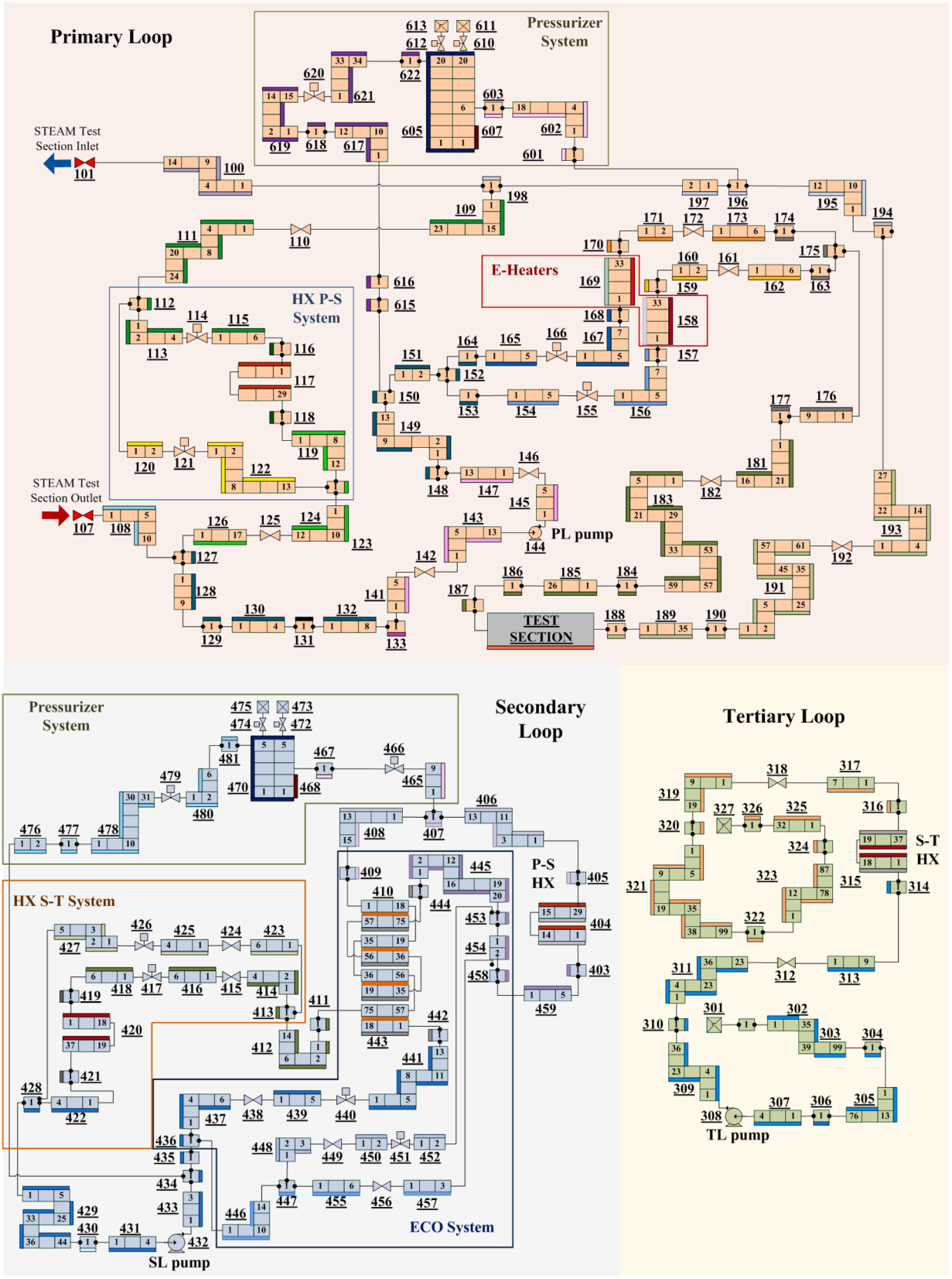

Fig. 4. Relap5/Mod3.3 nodalization of the three loops of Water Loop facility.

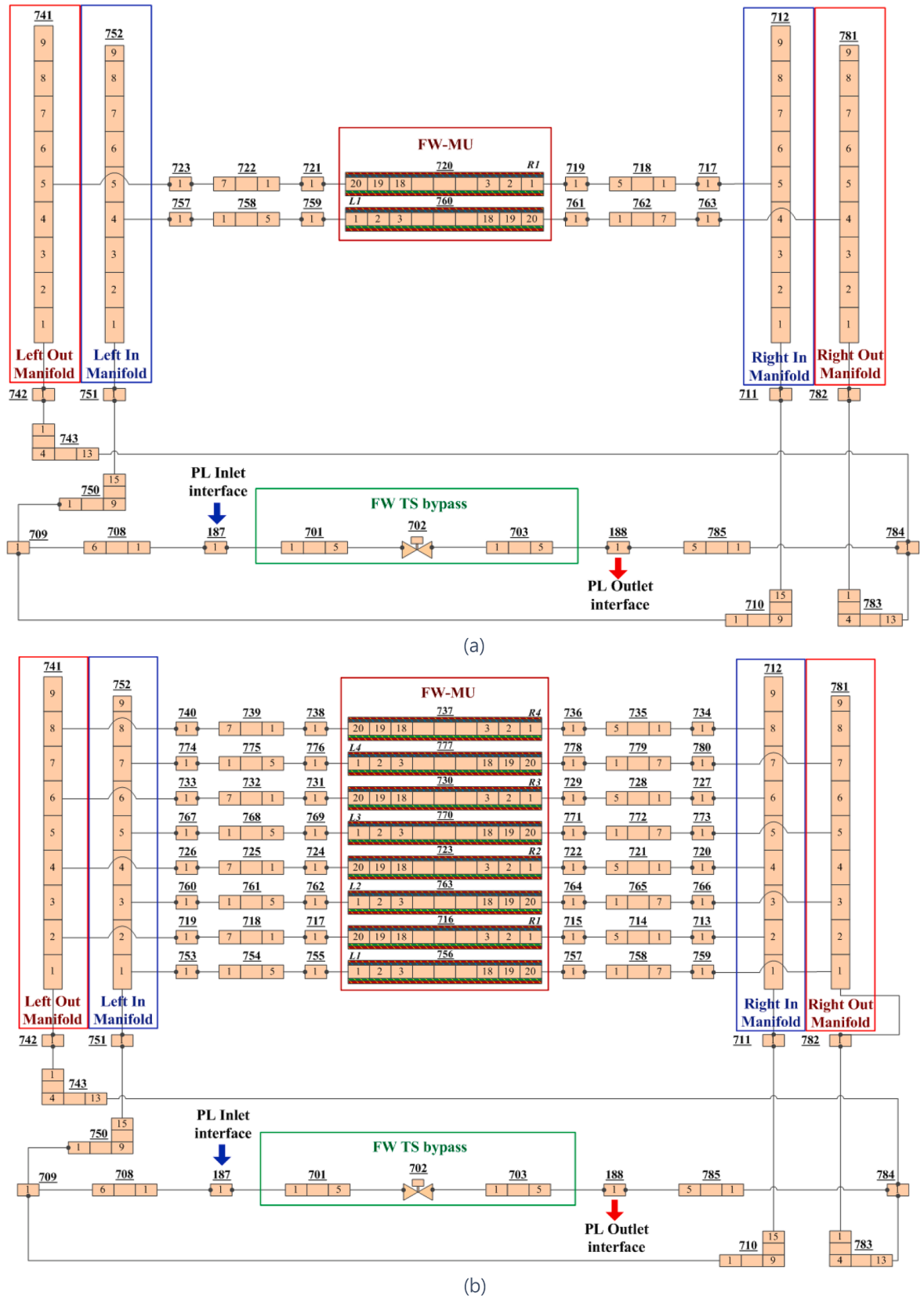

Fig. 5. (a): FW-TS Nodalization using a lumped approach. (b): WL-TS nodalization using a detailed approach.

Table 3
WL and FW-TS nodalization parameters.

Systems Parameters	Water Loop			First Wall Test Section		**TOTAL**	
	PL	SL	TL	Lumped model	Detailed model	Lumped model	Detailed model
Hyd. Volumes	918	495	539	183	398	2135	2350
Junctions	964	507	537	184	406	2192	2414
Heat Structures		2142		120	480	2262	2622
Mesh points		39,431		1440	5760	40,871	45,191

temperature at the fluid total pressure, single-phase liquid convection is predicted, and Dittus-Boelter correlation is applied [15]. For external flows over tube bundles, such as in the WL facility heat exchangers, enhanced turbulence is accounted for by multiplying the Dittus–Boelter result by the pitch-to-diameter-based turbulence correction factor developed by Inayatov [16]. Once the wall temperature exceeds the saturation temperature, nucleate boiling initiates. In this regime, RELAP5 adopts the Chen correlation [17]. When a significant amount of water is vaporized, the liquid film adjacent to the wall is progressively replaced by a vapor blanket, impeding heat transfer (dry-out). The corresponding heat flux is called Critical Heat Flux (CHF), and it is determined by the code using the 1986 Groeneveld look-up tables [18]. Beyond CHF, the heat transfer regime transitions to film boiling. And the system code evaluates the heat transfer coefficient as the greater of two correlations: the Chen transition boiling model [19], and the Bromley film boiling model corrected by Sudo [20,21].

Regarding the friction factor model associated with the distributed pressure drops, the Zigrang-Sylvester [22] approximation to the Colebrook correlation [23] is used as default one by RELAP5. If a two-phase mixture is present, the Lockhart-Martinelli multiplier is also considered [24,23].

3.1. Numerical model

3.1.1. Water Loop facility

The PL is modelled with volumes from 100 to 198, except for the pressurizer system, composed of the surge line, spray line, main tank and valve relief system, that is represented by components from 601 to 622. Since the PL is shared with STEAM facility, the volumes from 100 to 108 correspond to the STEAM branch, but for the following analyses this line is intercepted by means of the 101 and 107 valves. The P-S HX is modelled through pipe 117 which is provided with a HS that thermally couples PL and SL. The two regulation valves controlling the heat transfer are represented by the components 114 and 121. The cold leg is realized with volumes from 118 to 186, with branch 131 serving as the filter, and element 144 as the pump. The two electrical heaters are modelled by pipes 158 and 169. The 187 element represents the test section, which, for the present analysis, is characterized in Fig. 5. The hot leg is modelled by elements from 188 to 116 closing the loop. The only active HSs present in the PL nodalization are those modelling the pressurizer heater, and the electrical heaters resistances.

The SL is represented by elements from 403 to 481. Pipes 404, 410, 443 and 420 represent the P-S HX shell, the ECO shell and tubes, and the S-T HX tubes, respectively. The filter is identified by volume 430 and is followed by the SL pump with the number 432. The SL pressurizer system is modelled by components from 465 to 481, with the pressurizer itself being represented by pipes 468 and 470. The HS modeling the ECO tubes thermally couples the pipes 410 and 443, while the SL and TL are linked through the HS that represent the S-T HX tubes. In the SL nodalization, the only active HS present is the one modeling the pressurizer heater.

The TL, represented by elements from 300 to 327, is simplified and is conceived as an open circuit with an inlet and an outlet boundary condition. Components from 300 to 314 stand for the cold leg, with element 308 being the TL circulation pump. The S-T HX shell side is identified by pipe 315, and the remaining volumes represent the hot leg.

All the volumes of the three loops are provided with HSs that model the heat losses towards the environment. For each component, the design thermal insulation is also modelled.

3.1.2. First Wall test section

The FW-TS is modeled using two different approaches regarding the FW-MU portion: in the first approach (lumped approach) the eight countercurrent channels are represented by two lumped channels, i.e. the four channels in a given direction are collapsed into a single channel. Instead in the second approach (detailed approach) the eight channels are nodalized individually. These two nodalizations are compared in the steady state analysis, to evaluate differences in the results, and to select the one to be used in the NOS and LOFA test analysis.

The FW-TS, modelled by elements from 701 to 785, interfaces with the PL through volumes 187 and 188. Pipes 701 and 703 represent the TS bypass, and element 702 is the bypass regulating valve. The inlet and outlet manifolds are represented by vertical pipes, each consisting of 9 volumes, modeled using the slice nodalization technique. This approach involves vertically segmenting the entire system to ensure consistent mesh length for vertical control volumes across different nodalization regions aligned at the same axial level to improve the capability of the code to reproduce natural circulation [25]. The FW-MU is connected to the four manifolds by means of circular tubes modelled by two branches and one pipe in both directions. In the lumped approach, the FW-MU is modelled by two countercurrent pipes (i.e. 720 and 760) representing 4 collapsed channels each, connected with the manifolds at an average elevation between those of the corresponding channels. In the detailed approach the FW-MU is modelled by eight channels (i.e. 756, 716, 763, 723, 770,730, 777, 737), alternatively connected with the right and left inlet manifolds with a pitch of 22.5 mm. The channels are denoted using an abbreviation that specifies the inlet side, either *R* for right or *L* for left, followed by a number. The numbering progresses from bottom to top on both sides. The concentrated pressure drops coefficient of the diverging tees and of the manifolds junctions were evaluated accordingly to the formulas indicated in the Idelchick handbook of hydraulic resistance [26]. In both nodalizations the FW-MU channels are represented by 20-volumes pipes with the first and last two volumes corresponding to the flattened FW elbows, while the remaining 16 volumes represent the flat toroidal section. Each squared channel is provided with three HS: the first represents the front slab, which is exposed to the incident EB-Gun thermal flux; the second represents the back slab, subjected to the thermal flux of the back haters; and the third represents the heat transfer problem between adjacent channels in the poloidal direction (to simulate the countercurrent flow configuration). To reproduce the heat flux distribution on the lateral sections of the FW-MU, an average value of the sinusoidal trend is applied to the corresponding HSs.

3.2. Steady states at different power levels

Before performing the pre-tests of NOS and LOFA, it is first necessary to select the optimal FW-TS nodalization by comparing the proposed ones. This is done by evaluating the thermal-hydraulic performances of both models, under flat top conditions, considering 100%, 50% and 25% of the maximum pulse power and heat fluxes listed in Table 2. The main thermal-hydraulic parameters of the resulting six analyses are listed in Table 4 together with the simulation and computational times of the

Table 4
Test matrix of the steady state numerical analyses.

	Analysis n°					
Parameter	**1**	**2**	**3**	**4**	**5**	**6**
Nodalization		Detailed			Lumped	
Simulation time [s]	4.00e+3	4.00e+3	4.00e+3	4.00e+3	4.00e+3	4.00e+3
Computetional time [s]	2.08e+4	2.08e+4	2.08e+4	1.94e+3	1.94e+3	1.94e+3
Power [kW]	204.4	102.2	51.1	204.4	102.2	51.1
Power [%]	100	50	25	100	50	25
Pressure at pressurizer [MPa]		15.5			15.5	
Inlet Temperature [°C]		295			295	
Mass flow rate [kg/s]		1.047			1.047	
Max EB-gun heat flux [kW/m^2]	661.6	330.8	165.4	661.6	330.8	165.4
EB-gun heat flux elbows [kW/m^2]	498.4	249.2	124.6	498.4	249.2	124.6
Back heaters heat flux [kW/m^2]	90.02	45.01	22.5	90.02	45.01	22.5

analyses.

For the different power levels, the absolute pressure trend in the FW-TS for the detailed nodalization is illustrated in Fig. 6, while Table 5 provides the pressure drops distribution across all six analyses. The pressure observed at the FW-TS is higher than the one imposed at the pressurizer, as listed in Table 4. This is due to hydrostatic head, since the VC, where the FW-TS is installed, is located at the lowest point of the facility. Considering the detailed nodalization, different flow paths in parallel are available to evaluate the pressure drops. Among them, the selected is the one related to channel R1. Instead, for the lumped nodalization, only two flow parallel flow paths can be individuated. The chosen is the right one. The circled numbers shown in Fig. 6 correspond to the different sections of the FW-TS listed in Table 5.

The graph indicates that the TS pressure drops are mostly concentrated in the FW-MU channels, and that generally increase with higher power level. A slight pressure rise is observed in the first pipe section (#1) due to the elevation decrease at the TS inlet. For the same reason, the pressure differences in the inlet manifold (#3) and outlet manifold (#7) exhibit a noticeable difference. In the inlet manifold, the change in height results in a pressure decrease, while in the outlet manifold, it causes a pressure increase. Table 5 demonstrates that the primary contributors to the pressure drops, aside from the FW-MU, are the two connecting tubes linked to the inlet and outlet manifolds (#2 and #8). Additionally, at equivalent power levels, the total pressure drops between the two nodalizations differ by less than 2%.

Fig. 7(a) and (b) illustrates the temperature and the mass flow rate distributions over the eight channels for the detailed nodalization. Specifically, the parameters $\sigma_{\Delta T}$ and σ_{MFR} were used to characterize the dispersion of these quantities, and to compare the different power levels:

$$\sigma^i_{\Delta T} = \frac{\left(T^i_{out} - T^{FW-TS}_{in}\right) - \left(T^{FW-TS}_{out} - T^{FW-TS}_{in}\right)}{\left(T^{FW-TS}_{out} - T^{FW-TS}_{in}\right)}\% \quad (1)$$

$$\sigma^i_{MFR} = \frac{MFR_{i,} - MFR_{ave}}{MFR_{ave}}\% \quad (2)$$

Where:

1. T_{in} is the inlet FW-TS temperature
2. T^i_{OUT} is the i-th channel or manifold outlet temperature
3. T^{FW-TS}_{OUT} is the outlet FW-TS temperature (after the mixing of the T^i_{OUT}).
4. MFR_i is the i-th channel or manifold mass flow rate
5. MFR_{ave} is the average channel or manifold mass flow rate

The graph shows that, on average, the left channels display higher mass flow rates and consequently lower outlet temperatures compared to the corresponding right channels. This disparity may be attributed to the slightly lower elevation of the left channels, resulting in shorter flow paths for the fluid. Additionally, it is evident that the central channels on both sides (i.e., L2, L3, R2, R3) are the most disadvantaged, possibly as a result of the concentrated pressure drops applied in the manifolds junctions. Furthermore, as power levels increase, the lower channels (i.e., L1, L2, R1, R2) demonstrate a rise in flow rate to the detriment of the upper channels (i.e., L3, L4, R3, R4), leading to an inverse effect on the outlet temperatures. This behavior may be associated with increased pressure drops caused by higher fluid densities, which exert greater influence along longer flow paths.

Table 6 provides a comparison of the two proposed nodalizations for

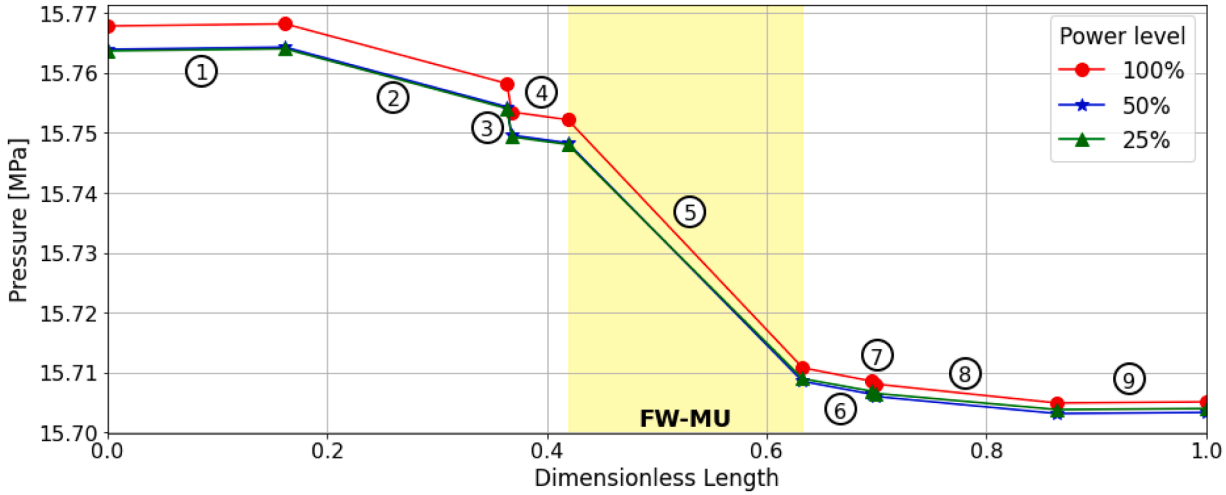

Fig. 6. Pressure distribution over the FW-TS for the detailed nodalization at different power levels.

Table 5
Comparison of pressure drops distribution over the FW-TS for the detailed and the lumped nodalization.

		Analysis n°					
		1	2	3	4	5	6
#	Element	Pressure Drops [kPa] *(% on total)*					
1	Pre-bifurcation pipe	0.3 *(0.4)*	0.3 *(0.5)*	0.3 *(0.5)*	0.3 *(0.4)*	0.3 *(0.5)*	0.3 *(0.5)*
2	Post-bifurcation pipe	6.2 *(9.9)*	6.2 *(10.3)*	6.2 *(10.4)*	6.2 *(9.8)*	6.2 *(10.1)*	6.2 *(10.3)*
3	Inlet Manifold	3.4 *(5.4)*	3.4 *(5.6)*	3.4 *(5.7)*	3.8 *(6.0)*	3.8 *(6.2)*	3.8 *(6.3)*
4	Inlet circular channel	1.3 *(2.1)*	1.3 *(2.1)*	1.3 *(2.2)*	1.3 *(2.0)*	1.3 *(2.1)*	1.3 *(2.2)*
5	**FW-MU**	**41.2*(66.0)***	**39.7*(65.9)***	**39.1*(65.8)***	**41.0*(64.6)***	**39.6*(64.8)***	**39.0*(64.7)***
6	Outlet circular channel	2.2 *(3.6)*	2.1 *(3.5)*	2.0 *(3.4)*	2.3 *(3.5)*	2.1 *(3.5)*	2.1 *(3.4)*
7	Outlet Manifold	1.9 *(3.1)*	1.8 *(3.0)*	1.8 *(3.0)*	2.7 *(4.3)*	2.3 *(3.7)*	2.1 *(3.7)*
8	Pre-reunification pipe	5.7 *(9.1)*	5.4 *(8.9)*	5.2 *(8.8)*	5.7 *(9.0)*	5.4 *(8.8)*	5.2 *(8.7)*
9	Post-reunification pipe	0.2 *(0.3)*	0.2 *(0.3)*	0.2 *(0.3)*	0.2 *(0.3)*	0.2 *(0.3)*	0.2 *(0.3)*
TOTAL		**62.42**	**60.31**	**59.39**	**63.42**	**61.13**	**60.26**

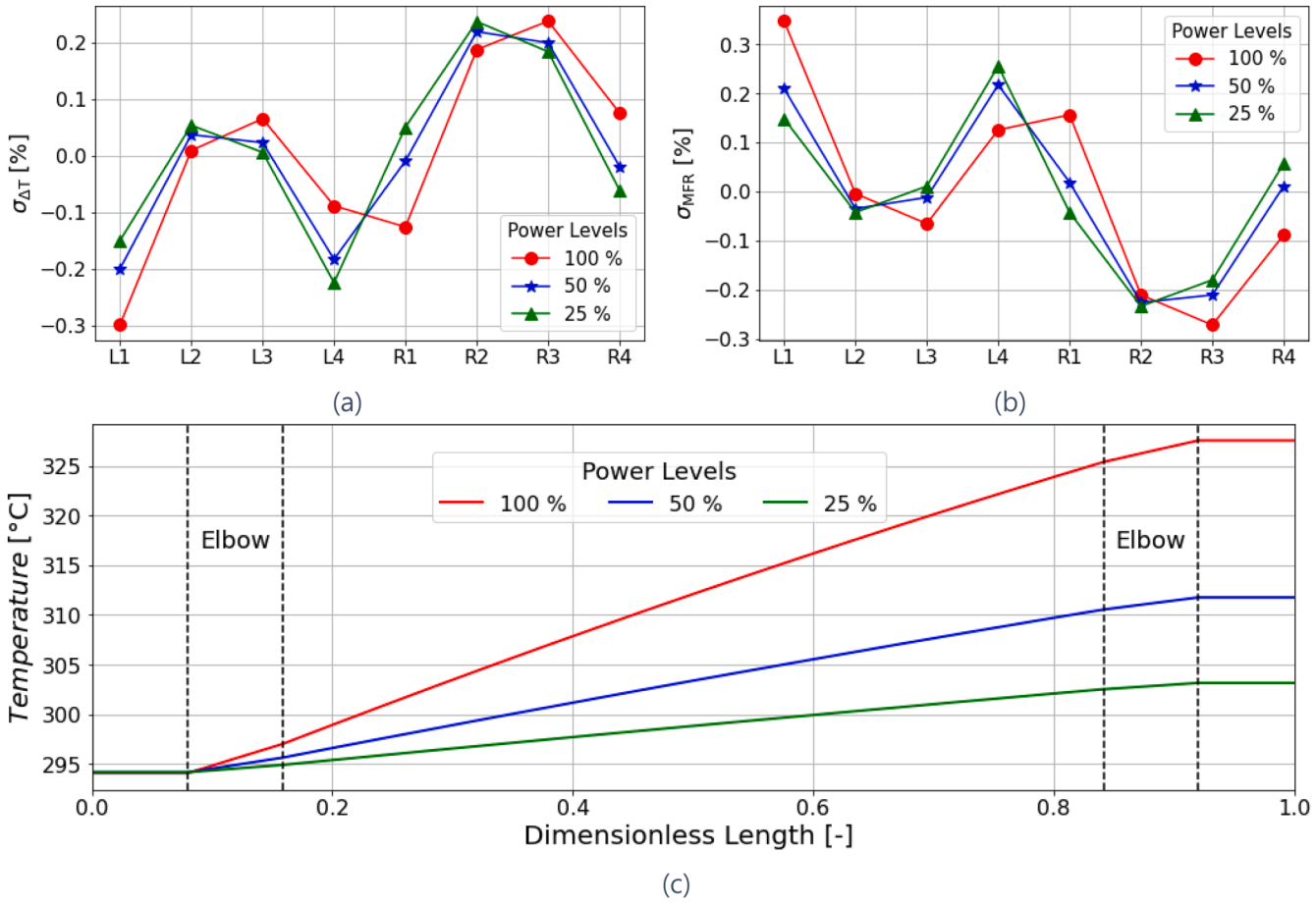

Fig. 7. (a) $\sigma^i_{\Delta T}$ of the FW-MU channels at different power levels; (b) σ^i_{MFR} of the FW-MU channels at different power levels; (c) Temperature profile of the R1 channel of the FW-MU at different power levels.

the 100% power level case (i.e., Analysis 1 and Analysis 4) focusing on the inlet/outlet temperature gradients across the channels, and mass flow rate distribution. The table indicates that mass flow rates and temperature differences along the left and right sides of the two nodalizations are closely aligned. The same deviation is observed, with the left side showing an advantage over the right one in terms of mass flow rate, thus determining a slight difference in terms of exit temperatures.

Fig. 7(c) shows the temperature profile over the R1 channel of the detailed nodalization of the FW-MU, at different power levels. The graph shows that the exit temperature decreases proportionally with the power level and that the profile is linear with the exception of the elbows. The difference in the heat flux determines a slope change in the temperature gradient.

The results presented in this section demonstrate that, both in terms of pressure drops, as shown in Table 5, and in terms of mass flow rate distribution and resulting thermal differences, as shown in Table 6, the two nodalizations provide comparable outcomes, with negligible deviations. However, for the subsequent analysis the detailed nodalization was selected to observe any potential asymmetrical behavior or instability between the distinct channels in transient conditions. This decision is further justified by the fact that, as shown in Table 4, the difference in computational time between the two nodalizations is about 7%.

Table 6
Comparison of $\sigma^i_{\Delta T}$ σ^i_{MFR} for the detailed and lumped nodalizations, at 100% power level.

		Analysis n°					
		1		4	1		4
		ΔT [K] ($\sigma_{\Delta T}$ [%])			MFR [kg/s] (σ_{MFR} [%])		
Channels	Right	1st	33.52 *(−0.13)*	33.59 (+0.10)	1st	0.1311 *(+0.16)*	0.5230 (−0.10)
		3rd	33.63 *(+0.24)*		3rd	0.1306 *(−0.21)*	
		2nd	33.64 *(+0.19)*		2nd	0.1305 *(−0.26)*	
		4th	33.59 *(+0.08)*		4th	0.1307 *(−0.10)*	
	Left	1st	33.46 *(−0.30)*	33.53 (−0.9)	1st	0.1313 *(+0.35)*	0.5240 (+0.10)
		3rd	33.57 *(+0.01)*		3rd	0.1309 *(+0.00)*	
		2nd	33.58 *(+0.07)*		2nd	0.1308 *(−0.06)*	
		4th	33.53 *(−0.09)*		4th	0.1310 *(+0.13)*	
Manifolds	Right	33.59 *(+0.09)*		33.59 (+0.10)	0.5230 *(−0.10)*		0.5230 (−0.10)
	Left	33.53 *(−0.08)*		33.53 (−0.9)	0.5240 *(+0.10)*		0.5240 (+0.10)
FW-TS		**33.56**		**33.56**	**1.047**		**1.047**

3.3. Power transitions

The power transitions under Normal Operation State conditions correspond to the Pulse-Dwell profile characteristic of the tokamak fusion reactor operation. The experimental test planned for the FW-MU in NOS conditions is designed to replicate this power profile by deflecting the EB-gun radiation and regulating the electrical back-heaters. In Table 7 the main characteristics of the NOS test power profile are presented [27]. The durations of the pulse and dwell phases and the ramp-up and ramp-down curves are aligned with the anticipated operation of the future DEMO reactor.

The PL is designed to provide the FW-TS with the thermal-hydraulic conditions specified in Table 7. A mass flow rate of 1.047 kg/s, required to sustain the correct thermal cycle in the pulse power condition, is controlled by the inverter-driven circulating pump of the PL, the power is then transferred to the SL via the P-S HX system and finally discharged to the TL via the S-T HX system. The Pressurizer system maintains the PL pressure at 15.5 MPa, while the FW-TS inlet temperature, regulated by both the P-S HX and electrical heaters, is maintained at 295 °C during both pulse and dwell phases.

The NOS pre-test numerical analysis was performed implementing the aforementioned control logics in the system and applying a heat transfer rate to the FW-MU front and back heat structures, mimicking the EB-Gun and back heaters power profile. The numerical simulation is constituted by two pulse-dwell cycles, starting from a pulse condition. The power source terms specific for the pulse and dwell phases are detailed in Table 8. The complete profiles of the EB-gun, back-heaters, and total power are illustrated in Fig. 8(a), the yellow and gray backgrounds indicate the pulse and dwell conditions, respectively. A closer view of these quantities, highlighting the transitions between pulse-dwell and dwell-pulse phases, is provided in Fig. 8(b), in which the ramp-up and ramp-down phases are highlighted in brown. This detailed representation reveals the shapes of the ramp-down and ramp-up curves: the former displays a linear trend, while the latter is distinguished by an initial peak before stabilizing at the nominal value. Fig. 8(c) shows the trends of the inlet and outlet FW-TS temperatures and the maximum structural temperature, localized on the front slab, over the same time interval. This graph demonstrates that the outlet and maximum structural temperatures follow the same trend as the power profiles, though with a delay caused by thermal inertia, which reduces the impact of the power peak observed at the end of the ramp-up phase. Additionally, during the pulse phase, the outlet temperature reaches the target value of 328 °C, while the maximum structural temperature remains below 343 °C, while both approach the inlet temperature of 295 °C in the dwell phase.

Table 7
Characteristic of the NOS pulse-dwell transitions [27], and thermal-hydraulic parameters.

NOS Pulse-Dwell characteristics	
Ramp-Up curve duration	150 s
Ramp-Down curve duration	150 s
Pulse duration	7200 s
Dwell duration	600 s
NOS test thermal-hydraulic parameters	
PL Mass flow rate	1.047 kg/s
PL Pressure	15.5 MPa
Inlet Temperature	295 °C

Table 8
NOS numerical analysis pulse specifications [9].

NOS numerical analysis specifications	Pulse	Dwell
EB-Gun power	178.9 kW	1.79 kW
Back heaters power	25.5 kW	0.26 kW
Total Power	204.4 kW	2.04 kW
EB-Gun maximum heat flux	661.6 kW/m^2	6.62 kW/m^2
EB-Gun elbows heat flux	498.4 kW/m^2	4.98 kW/m^2
Back heaters heat flux	90 kW/m^2	0.9 kW/m^2

3.4. Loss of flow scenarios

The LOFA scenario, explored for the WCLL BB, involves a significant reduction or interruption of the primary water coolant flow. Investigating this scenario is crucial, as it can lead to a rapid temperature rise in both the fluid and the blanket structure, posing a risk to system safety. In this context, the LOFA experimental tests planned for the FW-TS aims to evaluate the grace time and the system response to reduced mass flow to acquire valuable information about the current WCLL BB design safety features and to help the optimization of the incident management strategies.

To simulate the incidental scenario, thus the reduced mass flow rate conditions at the FW-TS, the regulating valve placed on the TS bypass line is employed. The partial opening of the valve reduces the flow reaching the FW-TS, so the severity of the LOFA scenario can be mimicked by changing the opening ratio.

The numerical analysis of these tests is based on the same principle, thus controlling the mass flow rate directed to the FW-TS by means of the bypass valve. Specifically, four LOFA tests were considered at 50%, 20%, 10%, and 5% of the nominal mass flow rate. To simulate the most severe accidental scenario, the Postulating Initiating Event (PIE) is set to occur in pulse condition, 10 s after the end of the ramp-up. The control logic introduced in the simulation includes a total shutdown of the EB-Gun and back heaters if the structure reaches the limit temperature of 550 °C, following a linear shutdown curve of 4 s.

Fig. 9(a) illustrates the flow rate supplied to the FW-TS over time. The background colors represent different phases: yellow for the pulse

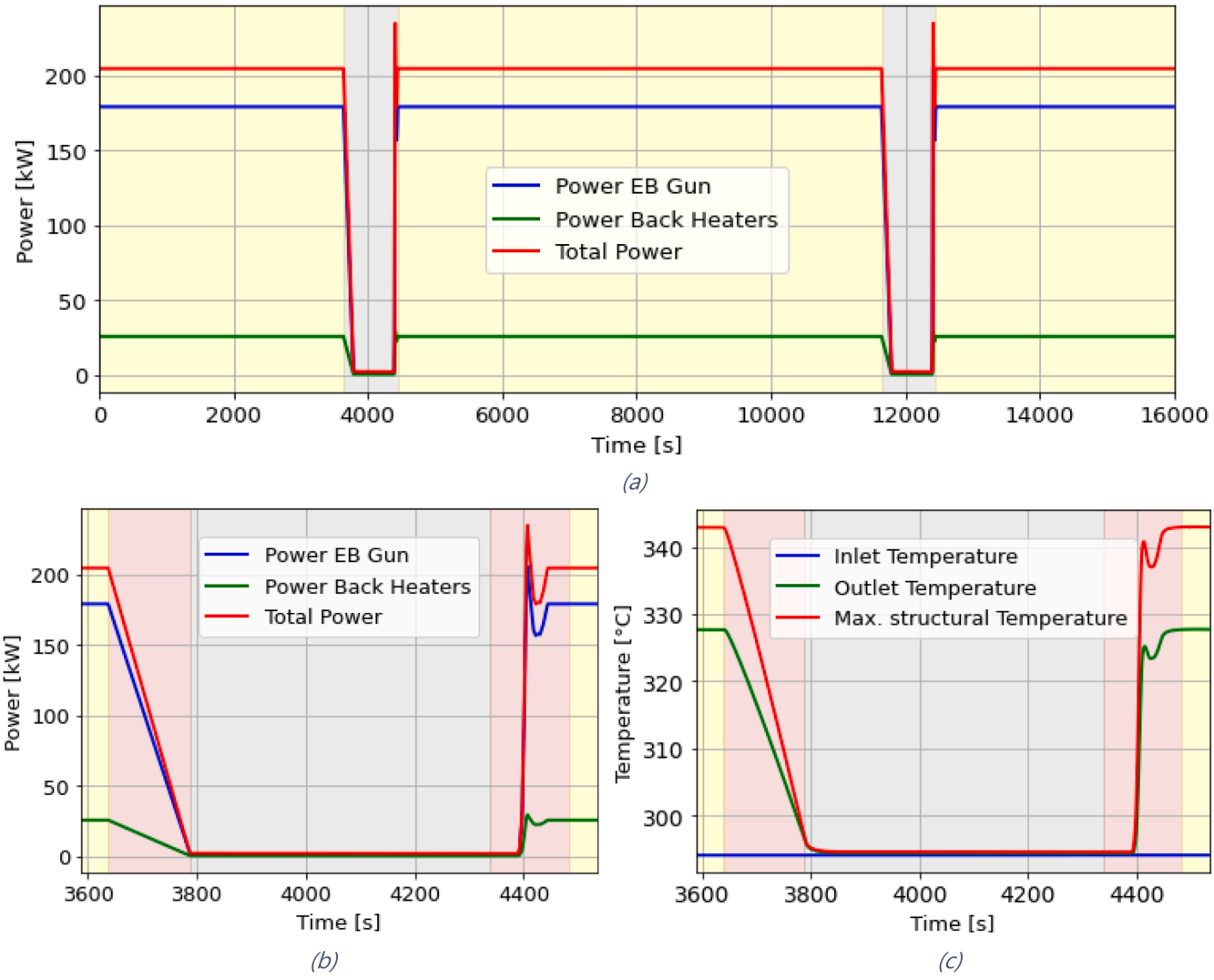

Fig. 8. (a) Pulse-dwell power profile of the numerical simulation; (b) Zoom of the Pulse-dwell power profile; (c) Zoom of the Pulse-dwell profiles of the inlet temperature, outlet temperature, and maximum structural temperature.

phase, brown for the ramp-up and ramp-down phases, and white for the LOFA test. The PIE is individuated with a black dashed line. The graph shows that following the test initiation and the opening of the control valve, the flow rate rapidly decreases to the target value. Steam formation in the FW-MU channels induces pressure drop variations in the circuit, leading to slight flow rate fluctuations. In Fig. 9(b) the σ^{i}_{MFR} of the different channels in the LOFA 5% test simulation is shown.

The graph shows that the LOFA condition determines a more dispersed mass flow rate distribution across the channels. The higher channels experience a disadvantage compared to the lower ones. Specifically, proceeding from the lower channel (L1) to the highest (R4), the mass flow rate ranges from a maximum that can reach up to a 30% increase above the average value, to a minimum that exceeds a 30% decrease. This phenomenon would not have been captured without the adoption of the detailed nodalization for the FW-MU, such decision is thus justified. Furthermore, in the following discussion reference will be made to channel R4, which is the most disadvantage one.

Fig. 10(a) presents the trend of the maximum structural temperatures recorded in the numerical simulations, providing a representation of the short-term response of the system. This graph outlines the peaks associated with the LOFA tests. The 50% mass flow rate reduction results in a structural temperature increase, though not enough to reach the limiting value of 550 °C. In the remaining cases, the control system is triggered, leading to the power cutoff and subsequent decline of the structural temperatures. In the mid/long-term the structure temperature approaches the inlet coolant temperature since no more power source is present. Additionally, the greater the mass flow rate reduction the faster is the rise in structural temperatures and, consequently, the shorter is the grace time. The 4-seconds shutdown curve determines a deposition of power to the FW-MU after the limiting temperature is reached. This results in exceeding 550 °C, with the extent of the exceedance increasing as the mass flow rate decreases. Table 9 collects the results of the numerical simulations in terms of grace time, maximum structural temperature and temporal extent of the temperature excursion. In the most critical condition, thus for the LOFA 5% test, the increment in the structural temperature above the limiting value of 550 °C lasts for 2 s and reaches a maximum of almost 5 °C, while the grace time is 13 s.

Fig. 10(b) and (c) show the outlet temperature and static quality of the R4, channel. The outlet temperature is evaluated as:

$$T_{out} = T^{g}_{out} X_{s,out} + T^{f}_{out} \left(1 - X_{s,out}\right) \quad (3)$$

Where:

1. T^{g}_{out} is the vapor phase outlet temperature
2. T^{f}_{out} is the liquid phase outlet temperature
3. $X_{s,out}$ is the outlet static quality

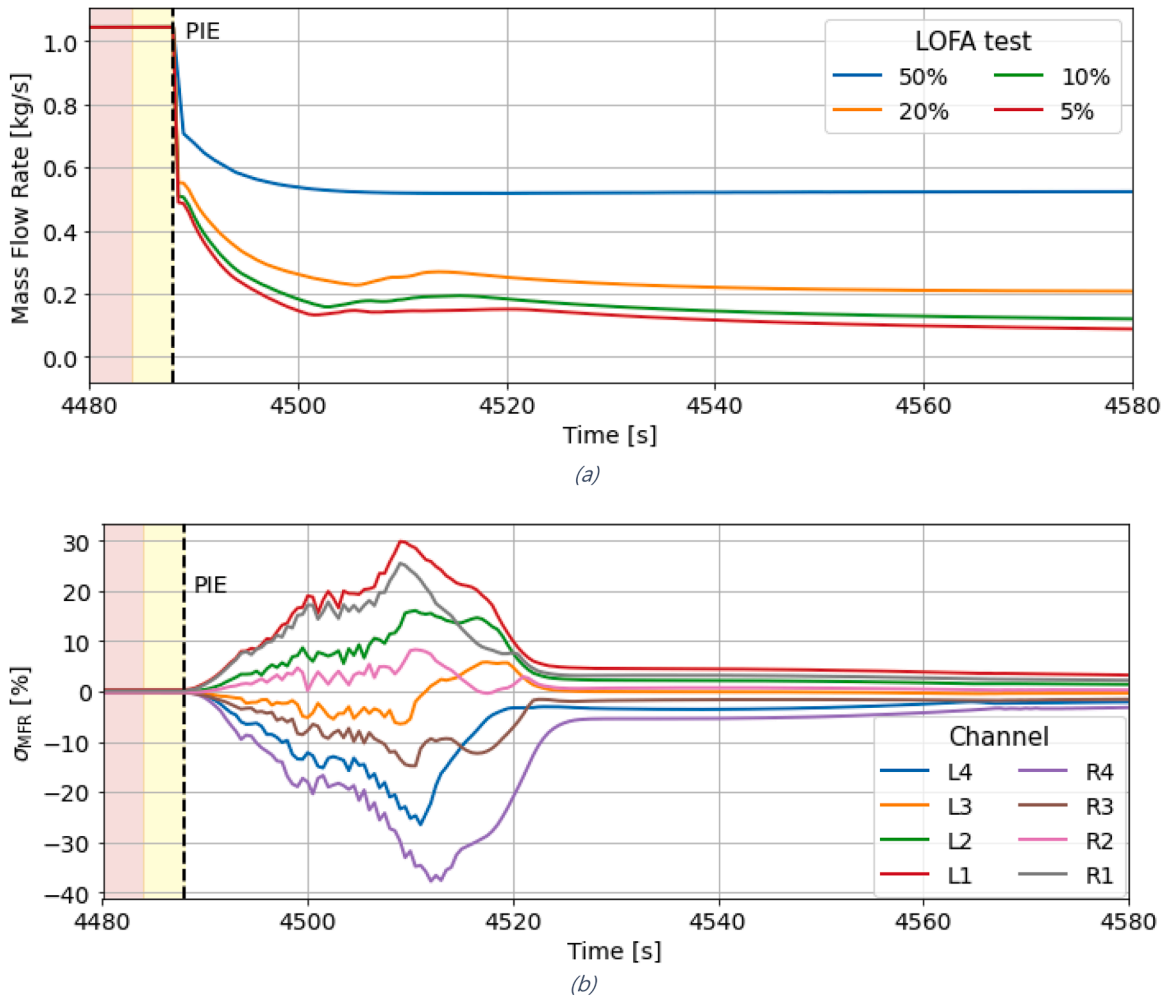

Fig. 9. (a) Mass flow rate evolution in the LOFA test simulations, (b) evolution of the σ^{i}_{MFR} of the FW-MU channels in the LOFA 5% test simulation.

The formula above is needed since RELAP5 is based on a non-homogeneous non-equilibrium two-phase model, solving six conservation equations (three for each phase, i.e., mass, momentum and energy). Consequently, the code does not compute a single temperature for the two-phase mixture but gives in output two values, one for the liquid and one for the vapor phase. The best way to obtain a single parameter representative of the two-phase mixture is to weigh the two temperatures by using the static quality, that is the quantity accounting for the relative mass presence of the two phases. In the LOFA50% simulation the saturation temperature is reached and there is limited steam production in Nucleate Boiling condition, with a static quality of approximately 0.1. In the remaining tests simulated, steam production is higher, becoming increasingly significant as the mass flow rate decreases, resulting in the LOFA5% simulation in a static quality of 0.6. As shown in Fig. 10(b), in the LOFA10% and LOFA5% simulations not only the saturation temperature is reached, but the produced steam also become superheated. Consequently, the outlet temperature reaches a maximum of 360 °C in the LOFA5% case, before the intervention of the control system.

In Fig. 11 the Critical Heat Flux Ratio (CHFR) over the R4 channel is represented using different colormaps for the different LOFA tests simulated. The CHFR is defined as the ratio between the CHF and the actual local heat flux, representing a safety margin against the thermal crisis. The vertical axis of each colormap represents the channel's axial direction, divided into the 20 vol that compose the FW-MU channels numerical model (see Section 3.1.2). The color scale swings from blue to red for decreasing CHFR, with white color indicating a CHFR less or equal to 1, signaling the occurrence of the thermal crisis. Black dashed horizontal lines mark the channel sections corresponding to elbows, which experience reduced heat flux. The CHF values computed in the code, as stated above, are based on Groeneveld Look-Up Table [18], which were specifically developed for circular channels. While this aspect introduces a limitation in the representativeness of the numerical results, it still provides valuable insights into the phenomenology. The LOFA50% simulation shows that halving the refrigerant mass flow rate determines a reduction in the CHF and, consequently, a decrease in CHFR. This condition stabilizes over time since there is no control system intervention. Additionally, the CHFR declines along the axial direction in relation to the increase in fluid temperature. This trend shifts at the outlet elbow, showing a slight rise in CHFR due to the reduction in heat flux. In the remaining simulations, the reduction in mass flow rate results in the occurrence of the thermal crisis defined by the departure from nucleate boiling. The thermal crisis, identified by the white areas, appears as a front that propagates down the length of the channel over time. At the outlet elbow this condition is mitigated, resulting in a split of the CHF propagation front into two distinct fronts, one moving from the channel's outlet volume, the other originating at the last volume with maximum thermal flux. This aspect is evident from the step observed in the white region at the penultimate volume across all three simulations. Comparing the LOFA20%, LOFA10% and LOFA5% colormaps reveal that the thermal crisis affects a larger portion of the channel with decreasing mass flow rate. In the LOFA10% and LOFA5%

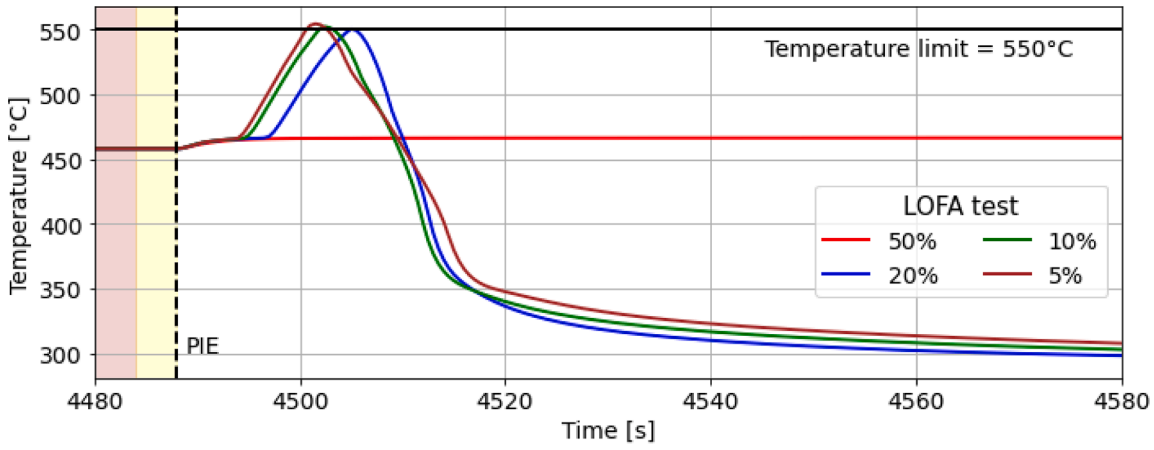

(a)

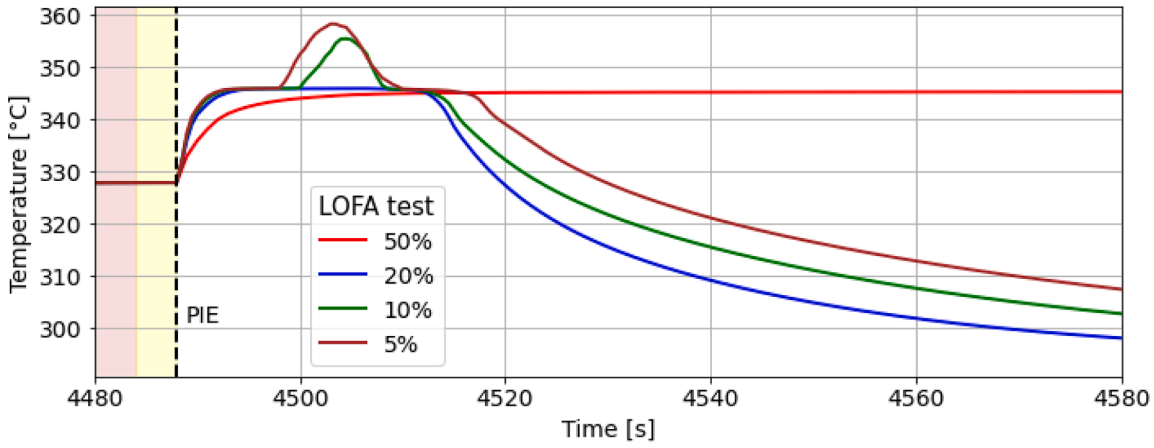

(b)

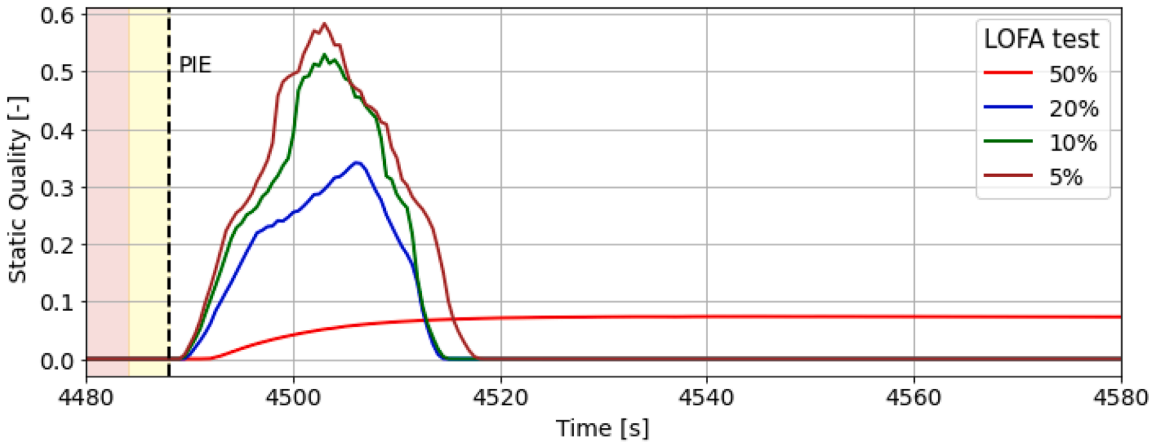

(c)

Fig. 10. (a) Maximum structural temperature over the FW-MU in the LOFA tests simulations; (b) Outlet temperature of the fluid at the outlet of the R4 channel in the LOFA tests simulation, (c) Outlet static quality at the outlet of the R4 channel in the LOFA tests simulation.

simulations, approximately 30% of the channel length is affected by departure from nucleate boiling conditions, for a maximum duration of about 10 s. This results in steam overheating at the outlet, as shown in Fig. 10(b). In the LOFA20% case, the thermal crisis impacts a very limited region in both time and space, insufficient to produce and sustain superheated steam.

4. Conclusions

In this paper the thermal-hydraulic performance of the WCLL BB FW mock-up under the experimental test conditions planned for the WL facility was investigated. A numerical model of the three loops composing the WL facility, along with the FW-TS was developed using the RELAP5/Mod3.3 thermal-hydraulic system code and the following

Table 9
Grace time and maximum structural temperature of the LOFA test simulations.

Test ID	MFR [kg/s]	Grace Time [s]	Period of Temperature excursion [s]	Max. structural T [°C]
LOFA50%	0.524	\	\	466.4
LOFA20%	0.2096	17	0.5	550.7
LOFA10%	0.1048	14	1.5	551.3
LOFA5%	0.0524	13	2	554.7

analyses were carried out.

A sensitivity analysis of the FW-TS nodalization was performed under steady state conditions. It showed that detailed and lumped nodalizations yield comparable results in terms of pressure drop distribution across the FW-TS, with the FW-MU channels playing the main role. Furthermore, the two nodalizations produced the same FW-TS outlet temperature. However, the mass flow rate distribution over the channels obtained using the detailed nodalization suggested its adoption for subsequent analyses as it presents an advantage in capturing potential asymmetries and instabilities.

The analysis of power transitions demonstrated that the FW-TS outlet temperature and structural temperature profiles are in line with the pulse-dwell operating conditions, with the maximum structural temperature on the outlet of the FW-MU remaining below the limiting value of 550 °C.

Simulations of the loss of flow scenarios for the FW-TS revealed that a reduction in mass flow rate determines an increase in the structural temperature, potentially exceeding the limiting temperature. The grace time following the PIE was of the order of tens of seconds and decreased with more severe LOFA conditions. Additionally, the control logic implemented in the simulation, featuring a 4 s linear shutdown curve, determines an increase in the maximum material temperature above 550 °C. Furthermore, the analyses highlighted the occurrence of thermal crisis in channels experiencing a strong reduction in mass flow rate, leading to steam overheating at the FW-MU outlet. These findings suggest the implementation of a more effective control system to prevent overheating and damage during the experimental tests, possibly by adopting a lower temperature limit for the control system intervention, or a faster shutdown curve. The choice of the structural temperature at which the shutdown should be triggered can be estimated by further numerical simulations using the model presented in this paper. However, the magnitude and duration of the temperature exceedance are so limited that they are not expected to pose a threat to the integrity of the

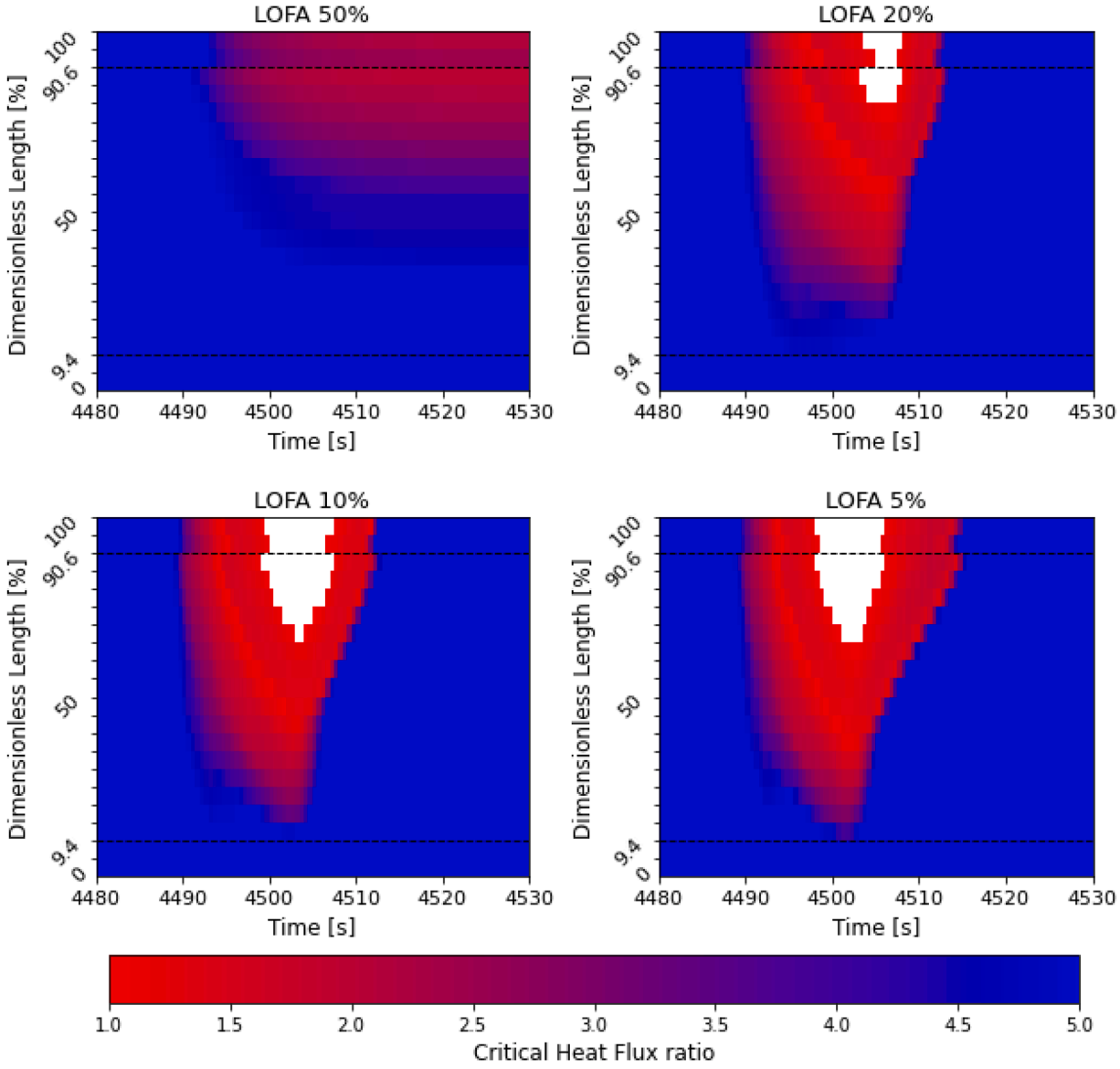

Fig. 11. Critical heat flux ratio over the FW-MU in the LOFA tests simulations.

materials.

The outcome of the present paper provides room for further developments. Additional analyses will be performed to investigate in more depth the LOFA scenario, aiming to identify the threshold mass flow rate reduction at which the limiting temperature is reached, and the thermal crisis occurs. Furthermore, the implementation of more accurate CHF correlations in the RELAP5 Mod3.3 code would enhance the representativeness of the numerical simulations compared with the experimental tests.

In conclusion these analyses offer valuable insight into WL facility operation and in the FW-TS thermal-hydraulic performance for the planned experimental tests. Comparing the numerical results with the experimental data, once available, will also be meaningful for code validation purposes.

CRediT authorship contribution statement

G. Mongiardini: Writing – original draft, Software, Methodology, Investigation, Formal analysis, Conceptualization. **A. Vannoni:** Writing – review & editing, Supervision, Methodology, Conceptualization. **C. Ciurluini:** Writing – review & editing, Supervision, Methodology, Conceptualization. **P. Maccari:** Writing – review & editing, Supervision, Methodology, Conceptualization. **B. Gonfiotti:** Writing – review & editing, Supervision, Methodology, Conceptualization. **P. Arena:** Writing – review & editing, Supervision, Conceptualization. **M. Eboli:** Writing – review & editing, Supervision, Conceptualization. **F. Giannetti:** Writing – review & editing, Supervision, Conceptualization. **A. Del Nevo:** Writing – review & editing, Supervision, Conceptualization.

Declaration of competing interest

The authors declare that they have no known competing financial interests or personal relationships that could have appeared to influence the work reported in this paper.

Acknowledgements

This work has been carried out within the framework of the EUROfusion Consortium, funded by the European Union via the Euratom Research and Training Programme (Grant Agreement No 101052200 EUROfusion). Views and opinions expressed are however those of the author(s) only and do not necessarily reflect those of the European Union or the European Commission. Neither the European Union nor the European Commission can be held responsible for them.

Data availability

Data will be made available on request.

References

[1] https://www.iter.org. last visited: 10/12/2024.
[2] C. Bachmann, et al., Re-design of EU DEMO with a low aspect ratio, Fusion Eng. Des. 204 (2024) 114518, https://doi.org/10.1016/j.fusengdes.2024.114518.
[3] https://euro-fusion.org/. last visited: 10/12/2024.
[4] G. Federici, et al., An overview of the EU breeding blanket design strategy as an integral part of the DEMO design effort, Fusion Eng. Des. 141 (2019) 30–42, https://doi.org/10.1016/j.fusengdes.2019.01.141.
[5] F. Maviglia, et al., Integrated design strategy for EU-DEMO first wall protection from plasma transients, Fusion Eng. Des. 177 (2022) 113067, https://doi.org/10.1016/j.fusengdes.2022.113067.
[6] P. Arena, et al., Design and integration of the EU-DEMO water-cooled lead lithium breeding blanket, Energies 16 (2023) 2069, https://doi.org/10.3390/en16042069.
[7] P. Arena, et al., W-HYDRA: a new experimental platform for the water-cooled lead lithium breeding blanket, Nucl. Fusion 64 (2024) 076043, https://doi.org/10.1088/1741-4326/ad50e9.
[8] A. Vannoni, et al., The design of water loop facility for supporting the WCLL breeding blanket technology and safety, Energies 16 (2023) 7746, https://doi.org/10.3390/en16237746.
[9] P. Maccari, Design of a prototypical mock-up for the experimental investigation of WCLL first-wall performances, Energies 16 (2023) 1685, https://doi.org/10.3390/en16041685.
[10] The US Nuclear Regulatory Commission (USNRC), RELAP5/MOD3.3 Code Manual Volume 1: Code Structure, System Models, and Solution Methods, NUREG/CR-5535, USNRC, Washington, DC, USA, 1995.
[11] A. Vannoni, et al., RELAP5-based thermal-hydraulic assessment of the STEAM facility for DEMO WCLL balance of plant analysis, Fusion Eng. Des. 202 (2024) 114397, https://doi.org/10.1016/j.fusengdes.2024.114397.
[12] M. Eboli, et al., PbLi/water reaction: experimental campaign and modeling advancements in WPBB EUROfusion project, Energies 16 (2023) 7729, https://doi.org/10.3390/en16237729.
[13] F. Edemetti, et al., Optimization of the first wall cooling system for the DEMO WCLL blanket, Fusion Eng. Des. 161 (2020) 111903, https://doi.org/10.1016/j.fusengdes.2020.111903.
[14] The US Nuclear Regulatory Commission, RELAP5/MOD3.3 Code Manual Volume 4, Models and Correlations, NUREG/CR-5535, USNRC, Washington, DC, USA, 2006.
[15] F.W. Dittus, L.M.K. Boelter, Heat transfer in automobile radiators of the tubular type, Publ. Eng. 2 (1930) 443–461.
[16] A.Y. Inayatov, Correlation of data on heat transfer flow parallel to tube bundles at relative tube pitches of $1.1 < s/d < 1.6$, Heat Transf. Sov. Res. 7 (3) (1975) 84–88.
[17] J.C. Chen, A correlation for boiling heat transfer to saturated fluids in convective flow, Process Des. Dev. 5 (1966) 322–327, https://doi.org/10.2172/4636495.
[18] D.C. Groeneveld, 1986 AECL-UO critical heat flux lookup table, Heat Transf. Eng. 7 (1–2) (1986) 46–62, https://doi.org/10.1080/01457638608939644.
[19] J.C. Chen, et al.,. A phenomenological correlation for post-CHF heat transfer. 1977, NUREG-0237.
[20] L.A. Bromley, Heat transfer in stable film boiling, Chem. Eng. Prog. 46 (1950) 221–227.
[21] Y. Sudo, Film boiling heat transfer during reflood phase in postulated PWR loss-of-coolant accident, J. Nucl. Sci. Technol. 17 (7) (1980) 516–530.
[22] D.J. Zigrang, N.D. Sylvester, A review of explicit friction factor equations, Trans. ASME J. Energy Resour. Technol. 107 (1985) 280–283.
[23] C.F. Colebrook, C.M. White, Experiments with fluid friction in roughened pipes, Proc. R. Soc. Lond. Ser. A Math. Phys. Sci. 161 (906) (1937) 367–381.
[24] R.W. Lockhart, R.C. Martinelli, Proposed correlation of data for isothermal two-phase, two-component flow in pipes, Chem. Eng. Prog. 45 (1) (1949) 39–48.
[25] F. Mascari, et al., Sensitivity analysis of the MASLWR helical coil steam generator using TRACE, Nucl. Eng. Des. 241 (4) (2011) 1137–1144, https://doi.org/10.1016/j.nucengdes.2010.05.002.
[26] I.E. Idelchik, Handbook of Hydraulic Resistance, 4th Revised and Augmented Edition, Begell House Inc., New Tork, 2008.
[27] L. Barucca, Maturation of critical technologies for the DEMO balance of plant systems, Fusion Eng. Des. 179 (2022) 113096, https://doi.org/10.1016/j.fusengdes.2022.113096.